Catalysis Today 175 (2011) 477–484

Contents lists available at ScienceDirect

Catalysis Today

journal homepage: www.elsevier.com/locate/cattod

Synthesis, characterization and catalytic performance of meso-microporous material Beta-SBA-15-supported NiMo catalysts for hydrodesulfurization of dibenzothiophene

Dengqian Zhang[a,b], Aijun Duan[a,*], Zhen Zhao[a,*], Xianqin Wang[c], Guiyuan Jiang[a], Jian Liu[a], Chengyin Wang[a], Mingcheng Jin[a]

[a] State Key Laboratory of Heavy Oil Processing, China University of Petroleum, Beijing 102249, PR China
[b] Research Institute of Petroleum Processing, SINOPEC, Beijing 100083, PR China
[c] Department of Chemical, Biological and Pharmaceutical Engineering, New Jersey Institute of Technology, Newark, NJ 07102, United States

ARTICLE INFO

Article history:
Received 15 October 2010
Received in revised form 25 February 2011
Accepted 30 March 2011
Available online 25 June 2011

Keywords:
Synthesis
Characterization
Hydrodesulfurization
Dibenzothiophene
Beta-SBA-15
Micro-mesoporous composite material
Catalysts

ABSTRACT

Micro-mesoporous composite material Beta-SBA-15 (BS) with the Beta structure and SBA-15 mesoporous structure was synthesized and used as catalyst support for hydrodesulfurization (HDS) of dibenzothiophene (DBT). The supports and catalysts were characterized by various techniques including XRD, nitrogen adsorption, SEM, TEM, ^{27}Al MAS NMR, and Pyridine-FTIR. The characterization results demonstrated that NiMo/BS had similar acidity to NiMo/Beta, and possessed more acid sites and stronger acidity than NiMo/SBA-15 and NiMo/Al_2O_3. Activity evaluation results showed that NiMo/BS exhibited the highest DBT HDS activity among all the catalysts that were studied, and the DBT conversion on NiMo/BS was about 1.6 times as much as that on NiMo/Al_2O_3 at weight time of 0.75 g min mol^{-1}. The better catalytic performance of NiMo/BS was attributed to the superiorities of the pore structure and large amounts of acid sites of micro-mesoporous BS.

© 2011 Elsevier B.V. All rights reserved.

1. Introduction

The sulfur content in transportation fuels should be deeply reduced by fuel regulation worldwide. Tier II regulations from US Environmental Protection Agency required that the sulfur specification of on-road diesel oil were lowered to 15 ppmw after June 2006, and the EU specification was expected to be below 50 ppmw in 2005 and was about 10 ppmw in 2010 [1,2]. To meet the stringent regulation of S content, even the highly refractory molecules such as dibenzothiophene (DBT) and 4,6-dimethyldibenzothiophene(4,6-DMDBT) must be desulfurized. Due to the effects of big molecule sizes and steric hindrance from the alkyl substituents, it is difficult to desulfurize DBT and 4,6-DMDBT by using the traditional hydrotreating catalysts. In order to remove these highly refractory molecules, several approaches have been pursued, among which the development of highly efficient support for HDS catalysts is of great importance [1].

Mesoporous materials with open pores are considered to be an ideal catalyst support candidates. For the catalytic conversion of large molecules, the large pore sizes of the mesoporous materials can mitigate the diffusion barrier for the reactants and the products. Mesoporous materials MCM-41 possess high surface area and ordered pores. These characteristics make it more suitable for acting as the support of HDS catalysts. MCM-41-supported CoMo catalysts were reported exhibiting higher activities for HDS of the refractory dibenzothiophenic sulfur compounds presented in light cycle oil (LCO), particularly 4,6-dimethyldibenzothiophene than the γ-Al_2O_3-supported one [3]. Souza et al. [4] prepared a series of CoMo/Al-MCM-41 catalysts with different Si/Al ratios in Al-MCM-41, and HDS results showed that the CoMo/Al-MCM-41 catalyst with Si/Al of 60 had the highest thiophene conversion. However, mesoporous material of MCM-41 has poor stability and relatively small pores (about 2–4 nm diameter), which can be easily blocked by HDS active phases. These disadvantages represent a serious limitation to the practical applications of MCM-41.

Compared with MCM-41, SBA-15 has a larger pores (about 5–10 nm in diameter), thicker pore walls and higher hydrothermal stability [5,6]. Sampieri et al. [7] prepared SBA-15 and MCM-41-supported MoS_2 catalysts with various Mo loadings. An average MoS_2 slab length of 2.8 nm and a stacking number of 2 were found

* Corresponding authors. Postal address: 18# Fuxue Road, Chang Ping District, Beijing 102249, China. Tel.: +86 10 89731586; fax: +86 10 69724721.
E-mail addresses: duanaijun@cup.edu.cn (A. Duan), zhenzhao@cup.edu.cn (Z. Zhao).

0920-5861/$ – see front matter © 2011 Elsevier B.V. All rights reserved.
doi:10.1016/j.cattod.2011.03.060

to be present in the pores of the SBA-15-supported catalyst. However, relatively small mesopores in the MCM-41 were blocked by MoS_2 slabs, resulting in its comparatively lower activity than that of the SBA-15-supported counterparts [7]. So mesoporous material SBA-15 has been utilized as the support for NiW [8], CoMo and NiMo [9] sulfides, and their hydrotreating activities have been explored using model compounds such as dibenzothiophene [8] and thiophene [9]. The above studies also proved the superior activities of SBA-15-supported catalysts than the conventional γ-Al_2O_3-supported catalysts.

However, just like MCM-41, pure siliceous SBA-15 material has an electronically neutral framework and is devoid of Brönsted and Lewis acid sites. This may be disadvantageous since suitable acidity of support can increase the conversion of the refractory molecules, especially for 4,6-DMDBT [10,11]. Many researchers tried to enhance the acidity of SBA-15 material by introduction of Al to the framework for the synthesis of Al-SBA-15 [12–14]. Although this introduction could adjust the acidy of the mesoporous materials, it still showed a lower acidity than zeolite, since the amorphous nature of the pore walls [15].

Recently, important advances toward the improvement of acidity and stability of mesoporous materials have been made through synthesis of micro-mesoporous composite materials [16,17]. Many kinds of micro-mesoporous materials including Y-MCM-41 [18], Beta-MCM-41 [19], and mesoporous ZSM-5 [20], were synthesized and applied in the field of catalysis. Sun and Prins [10] reported that the mesoporous ZSM-5-supported Pt, Pd and Pt–Pd catalysts exhibited much better catalytic performance for the HDS of 4,6-DMDBT than the conventional ZSM-5 or γ-Al_2O_3-supported ones. They also suggested that the further improvement in the catalytic performance can be expected by tuning the acidity and pore size of the mesoporous zeolites. Beta-MCM-41 was also used as a support to prepare the supported NiW HDS catalyst [19], and the catalyst showed higher catalytic activities than the pure Al_2O_3-supported one. Compared with Beta-MCM-41, micro-mesoporous material Beta-SBA-15 possesses the large-pore (>5 nm) mesostructure which can further enhance the diffusion of reactant and product molecules. This superior mass transfer property combined with the appropriate acidity make Beta-SBA-15 more suitable for HDS of refractory sulfur compounds.

In this work, novel Beta-SBA-15 composite material was successfully synthesized from zeolite Beta seeds by two-step hydrothermal crystallization method using Pluronic P123 triblock copolymer (EO_{20}–PO_{70}–EO_{20}) as the mesostructure directing agents. Beta-SBA-15-supported NiMo catalysts were prepared and tested for the HDS of DBT. Meanwhile, in order to clarify the effects of pore size and acidity of the support on the catalytic performance, other catalysts including Beta and SBA-15-supported NiMo catalysts were also prepared and evaluated. The physicochemical properties of pure supports and supported NiMo catalysts were characterized by various techniques, and their catalytic performances are compared with that of conventional NiMo/Al_2O_3 catalyst. The main factors affecting the catalytic performance of Beta-SBA-15 composite-supported NiMo catalyst for HDS of DBT are discussed.

2. Experimental

2.1. Preparation of the supports

2.1.1. Synthesis of Beta-SBA-15 (denoted as BS)

A zeolite seed solution was prepared by adding 0.19 g of NaOH, 0.76 g of $NaAlO_2$, and 21.43 g of tetraethylorthosilicate(TEOS) into 29.45 g of TEAOH aqueous solution (25%) to obtain a mixture of $Al_2O_3/SiO_2/Na_2O$/TEAOH/H_2O with a molar ratio of 1.0/30/1.4/15/360, and the mixture was then kept under agitation for 4 h at room temperature before being transferred into an autoclave to age for 24 h at 140 °C for obtaining zeolite Beta seed solution. 2 g of $EO_{20}PO_{70}EO_{20}$ (Pluronic P123) was dissolved in 62.5 g of 2 M hydrochloric acid at 40 °C. Finally, 4.3 g TEOS and 7.0 g of zeolite seed solution (containing 20 mmol of SiO_2) were mixed resulting in a mixture of Al_2O_3/SiO_2/P123/HCl/H_2O with a molar ratio of 1.0/60/0.52/188/10400. The mixture was maintained at 40 °C and stirred for 24 h and then transferred into an autoclave for further reactions at 100 °C for 24 h. The aluminosilicate precursor was collected by filtration, dried at 100 °C for 10 h, and calcined at 550 °C in air for 6 h to remove the templates.

2.1.2. Synthesis of Beta zeolite

Beta zeolite was prepared in the same way as the zeolite seeds described in the BS synthesis. The zeolite Beta was prepared by adding 0.19 g of NaOH, 0.38 g of $NaAlO_2$, and 21.43 g of tetraethylorthosilicate (TEOS) into 29.45 g of aqueous TEAOH solution (25%) to get a mixture of $Al_2O_3/SiO_2/Na_2O$/TEAOH/H_2O with a molar ratio of 1.0/60/1.4/15/360. The mixture was kept under stirring for 4 h at room temperature before being transferred into an autoclave for aging for 48 h at 140 °C to form zeolite Beta.

2.1.3. Synthesis of SBA-15

SBA-15 used in this work was synthesized using a method described elsewhere [5].

2.1.4. Preparation of H-Beta and H-BS

Beta and BS prepared previously were ion exchanged with 1.0 M NH_4Cl at 80 °C for 1 h before being washed with water and calcined at 550 °C in air for 4 h. The exchanging procedure was repeated twice to achieve the final products.

2.2. Preparation of the catalysts

The supported NiMo catalysts were obtained by two-step incipient-wetness impregnation method, and ammonium heptamolybdate and nickel nitrate were used as precursors for Ni and Mo, respectively. After each impregnation step, the samples were dried at 110 °C for 12 h, and calcined at 550 °C in air for 4 h. The loadings of Ni (NiO 3.5 wt%) and Mo (MoO_3 10 wt%) were kept the same in different catalysts.

2.3. Characterization of the supports and the catalysts

The composite supports and the catalysts were characterized by means of X-ray powder diffraction (XRD), Scanning electron microscopy (SEM), Transmission electron microscopy (TEM), N_2 adsorption, Fourier transform infrared spectroscopy with pyridine adsorption (Pyridine-FTIR), and ^{27}Al magic angle spinning nuclear magnetic resonance (^{27}Al MAS NMR).

XRD patterns were recorded in an XRD-6000 diffractometer at 40 kV using Cu Kα radiation. For wide angle scans, the 2θ range was from 20 to 80° (the diffractometer was operated at 30 mA), and for small angle scans, from 0.7 to 10° (the diffractometer was operated at 250 mA).

Surface areas and pore size distributions (PSD) of the samples were measured by nitrogen isotherms using a Micromeritics ASAP 2010 system. All the samples were degassed at 350 °C under vacuum prior to N_2 adsorption at −196 °C. The surface areas were calculated by using the BET model. The total volumes of micro- and mesopores were calculated from the amounts of nitrogen adsorbed at (P/P_0) of 0.98, assuming that adsorptions on the external surface were negligible compared with the adsorption in pores. The PSD were calculated by using the Barret–Joyner–Halenda (BJH) method. The micropores were determined from the *t*-plot analysis.

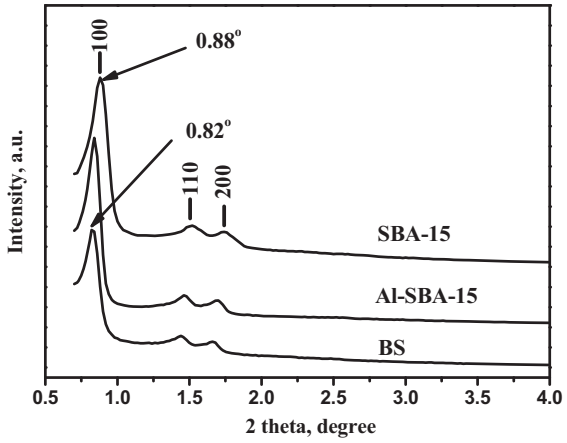

Fig. 1. XRD patterns of BS, Al-SBA-15, and SBA-15 samples in the small angle domain.

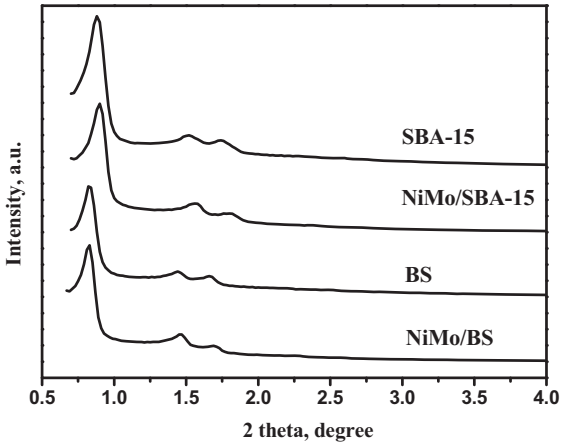

Fig. 3. XRD patterns of supports and catalysts in the small angle domain.

SEM images were obtained on a Cambridge S-360 apparatus operating at 20 kV. The silica-based samples were coated with gold before SEM measurement. TEM images were taken from thin edges of particles supported on a porous carbon grid using a Philips Tecnai G2 F20 equipment operating at 300 kV.

The nature of acid sites of the catalysts was determined by Pyridine-FTIR on a MAGNAIR 560 FTIR instrument (Nicolet Co., US) with a resolution of 1 cm^{-1}. The samples were dehydrated at 500 °C for 5 h under a vacuum of 1.33×10^{-3} Pa, followed by adsorption of purified pyridine vapor at room temperature for 20 min. The system was then degassed and evacuated at different temperatures, and the IR spectra were recorded.

^{27}Al MAS NMR spectra were recorded with a Bruker Avance III 500 MHz spectrometer. The ^{27}Al spectra were obtained at 130.327 MHz with a 0.9 μs pulse width, 6 μs delay time and 12 kHz spinning speed.

2.4. Catalytic activity measurement

The catalytic activities of the catalysts were studied by using DBT as the probe reactant, since its HDS process is a widely used model reaction for studying the deep HDS of diesel fuels. The reactions were carried out in a continuous fixed-bed inconel reactor (8 mm inner diameter and 400 mm in length) with 0.5 g catalyst (grain size of 0.3–0.5 mm). All catalysts were presulfided in situ with 2 wt% CS_2-cyclohexane and H_2 mixture at 360 °C and 4 MPa. The activity tests of DBT HDS were carried out under the conditions of 320 °C, 4.0 MPa, H_2/oil ratio of 200 mL mL^{-1}. Liquid reactant was fed to the reactor by a SZB-2 double-piston pump. The feed composition was 1.5 mmol cyclohexane (as solvent for the DBT), 0.004 mmol dibenzothiophene, and 53.8 mmol H_2. According to Ref. [21], a weight time was defined as $\tau = \omega cat/\eta feed$, where ωcat was the catalyst weight and $\eta feed$ was the total molar flow to the reactor. The weight time (τ) was changed by varying the flow rates of the liquid and the gaseous reactants with their ratio being kept at a constant value. All the reaction products were analyzed by offline Finnigan Trace GC/MS with a Trace Ultral gas chromatograph using a HP-5MS (30 m × 0.25 mm × 0.25 μm) capillary column and a pulsed flame photometric detector (PFPD).

3. Results and discussion

3.1. Structure of the supports and the catalysts

The XRD patterns of the synthesized samples are displayed in Figs. 1–4. As shown in Fig. 1, the SBA-15 sample shows an intense peak at $2\theta = 0.88°$ corresponding to the (1 0 0) plane, and two other peaks at $2\theta = 1.52°$ and 1.74° for (1 1 0) and (2 0 0) planes [5]. BS sample exhibits a sharp peak at $2\theta = 0.82°$, and followed by two other peaks. These peaks agreed well with the characteristics of SBA-15 structure, but possessed relatively low intensities and shifted to low angles. The lower intensities may be due to the presence of zeolite seeds in the synthesis process, which are more difficult to be assembled by the mesostructure directing agents and some assembled zeolite seeds [15]. Similarly, since the synthesis precursors contain zeolite seeds and primary building units, the size of

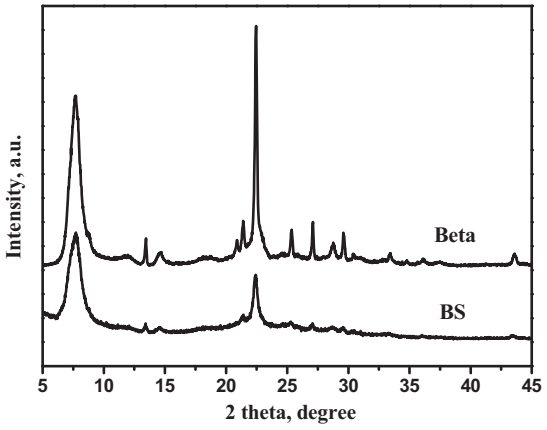

Fig. 2. XRD patterns of BS and Beta samples in the wide angle domain.

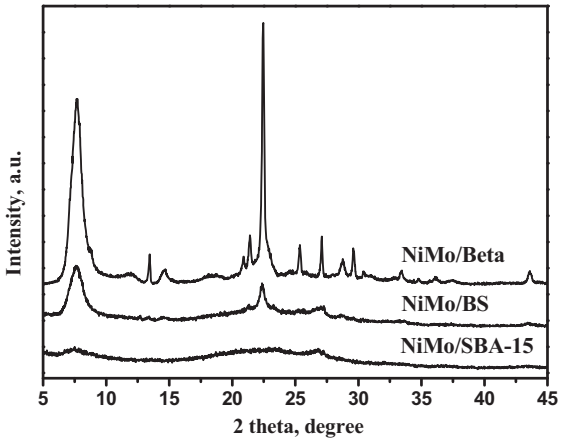

Fig. 4. XRD patterns of supported NiMo catalysts in the wide angle domain.

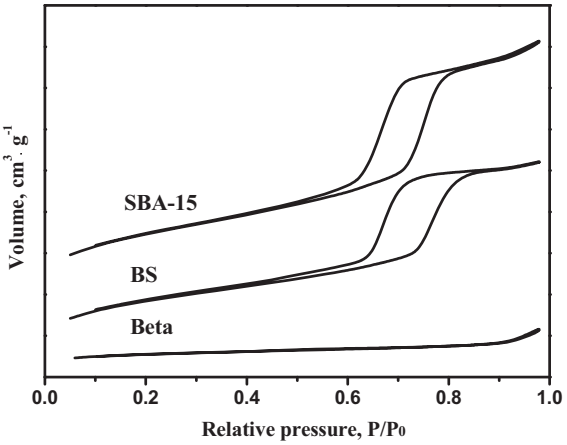

Fig. 5. Nitrogen adsorption/desorption isotherms of SBA-15, BS, and Beta samples.

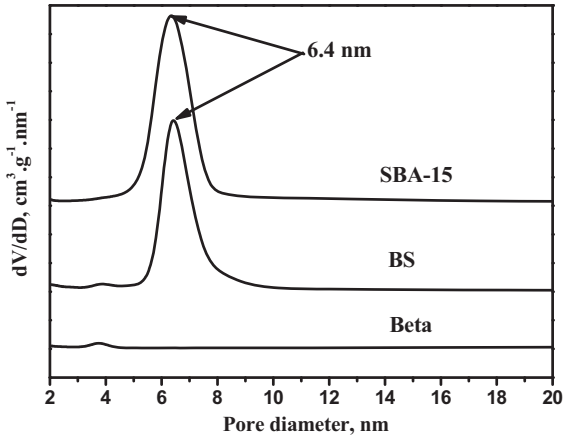

Fig. 7. Pore size distribution of SBA-15, BS, and Beta samples.

aluminosilicate precursor particles (zeolite seeds and primary units) should be larger than that of SiO_4 tetrahedrons for constructing the walls of mesopores. Moreover, both BS and Al-SBA-15 contain AlO_4 tetrahedron which has bigger size than that of SiO_4 tetrahedrons. As a consequence, the unit cell parameter of BS or Al-SBAS-15 should be bigger than that of pure silica SBA-15 which is assembled from SiO_4 tetrahedrons. So the diffraction peaks of BS and Al-SBA-15 shifted to low angles compared with pure silica SBA-15.

Fig. 2 shows the wide angle XRD patterns of the synthesized supports. Beta zeolite possesses very intense diffraction peaks at 7.6° and 22.4°, which is characteristic of zeolite Beta. BS sample also have the same diffraction peaks as zeolite Beta, but the peak intensities are relatively weak. Based on the XRD results, it is obvious that the as-synthesized material BS is the composite of SBA-15 and Beta zeolite.

Fig. 3 shows the small angle XRD patterns of the supported NiMo catalysts together with their corresponding supports. The XRD patterns clearly show that all catalysts (NiMo/BS, NiMo/SBA-15) keep the same structures as their corresponding supports. The results suggest that the mesoporous structure is retained even after active metal loadings. The wide XRD patterns for supported NiMo catalysts are shown in Fig. 4. The results reveal that MoO_3 is well dispersed on the supports since no MoO_3 peaks are detected. The absence of XRD signals indicates that the particle sizes of MoO_3 are below the coherence length of X-ray scattering, i.e., smaller than 3–4 nm [22].

3.2. Porous properties of the supports and the catalysts

The porous properties of the supports and the catalysts were examined by N_2 adsorption–desorption isotherms at −196°C. The textural and structural properties are shown in Table 1. The SBA-15 and BS supports possess high surface areas and pore volumes, which are consistent with the reported observations on mesoporous materials [5,23]. SBA-15 has micropores (V_{mic} = 0.09 $cm^3\ g^{-1}$) after the removal of triblock copolymers (the mesostructure template) that have been inserted into silicate walls [24]. BS has a relatively large V_{mic}/V_{mes} ratio because of the contribution of Beta zeolite. In addition, BS has a larger pore wall thickness than SBA-15. This is probably due to the stability of the mesoporous wall that is formed by assembling of the zeolite primary units (contained in the zeolite seed solution) and its lower tendency toward shrinkage during the decomposition of the template.

The textural characteristics of the supported NiMo catalysts show a significant decrease in surface area and pore volume after Ni and Mo are loaded on the supports (Table 1). Compared with the Al_2O_3-supported catalysts, this decrease is more pronounced for all the SiO_2-based supported catalysts. That can be attributed to pore blockage caused by a low dispersion of the active metal oxide phases according to the published report by Shimada et al. [25].

N_2 adsorption–desorption isotherms of the supports and the catalysts are shown in Figs. 5 and 6, respectively. All of SBA-15 and BS supports and their corresponding supported NiMo catalysts show the characteristic type-IV isotherms with H1-type hysteresis loop and a sharp capillary condensation step in the P/P_0 range

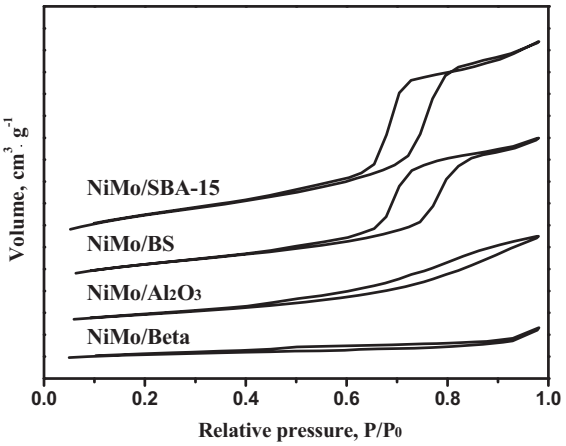

Fig. 6. Nitrogen adsorption/desorption isotherms of SBA-15, BS, Al_2O_3, and Beta-supported NiMo catalysts.

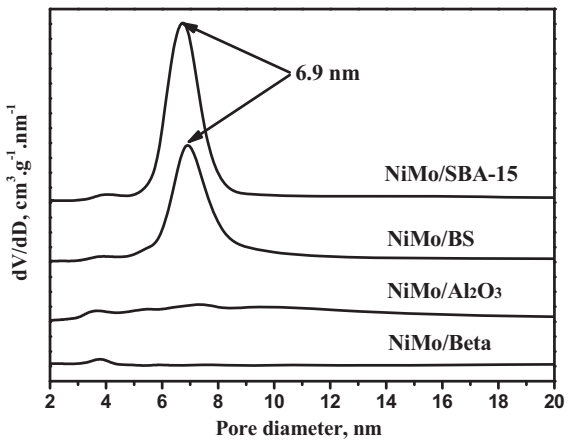

Fig. 8. Pore size distribution of SBA-15, BS, and Beta-supported NiMo catalysts.

Table 1
Textural properties of the supports and supported NiMo catalysts.

Samples	S_{BET}[a] ($m^2\ g^{-1}$)	V_t[b] ($cm^3\ g^{-1}$)	V_{mes}[c] ($cm^3\ g^{-1}$)	V_{mic}[d] ($cm^3\ g^{-1}$)	V_{mic}/V_{mes}	a_0[e] (nm)	d_{BJH}[f] (nm)	b_w[g] (nm)
SBA-15	699	1.03	0.99	0.09	0.09	11.6	6.4	5.2
BS	738	0.85	0.73	0.19	0.26	12.4	6.3	6.1
Beta	502	0.34	–	0.22	–	–	–	
Al_2O_3	207	0.48	0.50	–	–	–	3.9	–
NiMo/SBA-15	441	0.80	0.80	0.01	0.01	–	6.9	–
NiMo/BS	385	0.62	0.58	0.05	0.09		6.9	–
NiMo/Beta	339	0.26	–	0.15	–	–	–	–
NiMo/Al_2O_3	167	0.35	0.36	–	–	–	3.4	–

[a] Surface area was calculated by the BET method.
[b] The total pore volume was obtained at a relative pressure of 0.98.
[c] Mesopore volume was calculated using the BJH method.
[d] Micropore volume was calculated using the *t*-plot method.
[e] XRD unit cell parameter (a_0) was estimated from: $a_0 = d_{100} \times 2/3^{1/2}$ [5].
[f] d_{BJH} is the mesopore diameter calculated using the BJH method.
[g] b_w is the wall thickness evaluated according to Ref. [5]: $b_w = a_0 - d_{BJH}$.

of 0.6–0.8, a characteristic of large channel-like pores with a narrow pore size distribution (PSD). In contrast, the Beta support and the NiMo/Beta catalyst manifest their microporous properties with type I isotherms. Compared with the above materials, the Al_2O_3 support and the NiMo/Al_2O_3 catalyst show H4-type hysteresis loop with a small slope in the capillary condensation regime indicating a broad PSD. There is one thing in common for the adsorption–desorption isotherms of the different supports and their corresponding supported catalysts, i.e., no change is observed in the type of the isotherm and the shape of the hysteresis loop, which indicates that pore structure in the support is preserved after the deposition of active metals. The height of the hysteresis loop decreases after Ni and Mo loadings due to the reduction of the pore volume that results from metal deposition inside the mesopores (see Table 1).

The PSD of the supports and the supported NiMo catalysts are shown in Figs. 7 and 8, respectively. The BS and SBA-15 supports have a narrow PSD. Compared with the mesoporous materials, the Al_2O_3 support possesses a weak and broad PSD, whereas no mesopores are detected in the beta zeolite. Moreover, all of the catalysts show little change in the PSD when compared with their corresponding support.

3.3. Morphology of the supports

The SEM images of samples are shown in Fig. 9. The SBA-15 sample consists of many rice-like particles with a relatively uniform length of 1 μm. The BS sample consists of many vermicular-like domains, which are aggregated into wheat-like macrostructures. Beta zeolite showed the typical crystal particles with sizes ranging

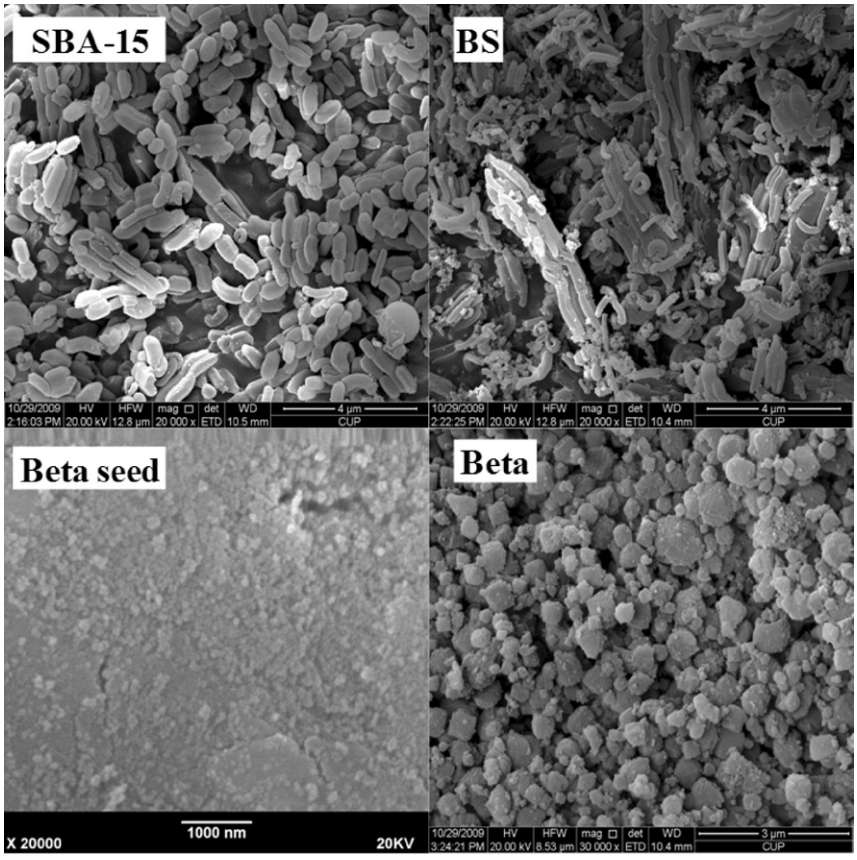

Fig. 9. SEM images of SBA-15, BS, Beta seed, and Beta samples.

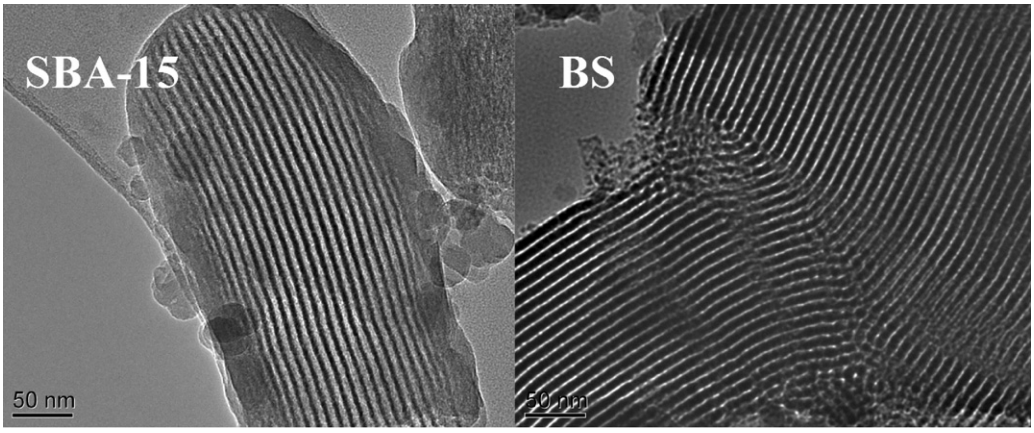

Fig. 10. TEM images of SBA-15, BS samples.

from 400 to 600 nm, and the Beta seed consists of fine particles which were aggregated into big block.

The TEM image (Fig. 10) of SBA-15 shows well-ordered hexagonal arrays of mesopores and confirms its 2D hexagonal structure with p6 mm symmetry [5,26]. Meanwhile, the TEM images of BS (in Fig. 10) show the same mesoporous channels as SBA-15, which confirm that both of SBA-15 and BS possess the 2D hexagonal p6 mm mesostructure. Their large pores (~7 nm) are clearly visible in the TEM images. These observations agree well with the results from N_2 adsorption and XRD.

3.4. Al coordination structures

^{27}Al MAS NMR spectra of Beta, BS, and Al-SBA-15 supports are shown in Fig. 11. The spectrum of zeolite Beta shows two sharp peaks. The intense peak at ~57 ppm is generally assigned to tetrahedral aluminum species (AlO_4 structural unit) which site in the framework of the zeolite [15,27]. The other signal at 0 ppm is attributed to octahedrally coordinated extra-framework aluminum species (AlO_6 structural unit). The low intensity at 0 ppm indicate that most of Al species are embedded into the zeolite framework. Similar phenomenon is observed in the BS. The chemical shift of tetrahedral aluminum in BS occurs at ~57 ppm rather than ~53 ppm, indicating that the framework aluminum species in BS is different from that in Al-incorporated mesoporous-silica materials (Al-SBA-15). A broad and weak peak at 0 ppm indicate that there are little extra-framework Al species presented in BS sample, which might be generated by the dissolution and dealumination of Beta zeolite seeds or the Beta primary units in the seed solution under the acidic condition during the synthesis of micro-mesoporous material. Al-SBA-15 shows only one peak at chemical shift of 53 ppm indicating that all the Al resources are embedded into the framework of mesoporous materials [28].

3.5. FT-IR spectra of the supports and the catalysts

In order to investigate the chemical bond connection in atomic level, we measured the IR spectra of SBA-15, Beta zeolite and BS (Fig. 12) and found that Beta zeolite and BS sample have very similar IR spectra. Two bands centered at ~524 and 571 cm^{-1} are observed in the FT-IR spectra of BS and Beta, which are typical vibration modes for zeolite Beta (six- or five membered rings of T–O–T (T = Si or Al) in microporous zeolites). These results may indicate that BS has the same structural unitand as Beta zeolite. In other words, in the atomic level the chemical bond connections in Beta zeolite and BS sample maybe very similar. This speculation is also supported by Al MAS NMR results (Fig. 11).

The acidities of the supported catalysts were investigated by Pyridine-FTIR method, and the spectra are shown in Figs. 13 and 14. Absorption bands due to adsorbed pyridine are observed in the spectra in the region of 1700–1400 cm^{-1}. According to the literature [29–31], the band at 1596 cm^{-1} can be assigned to

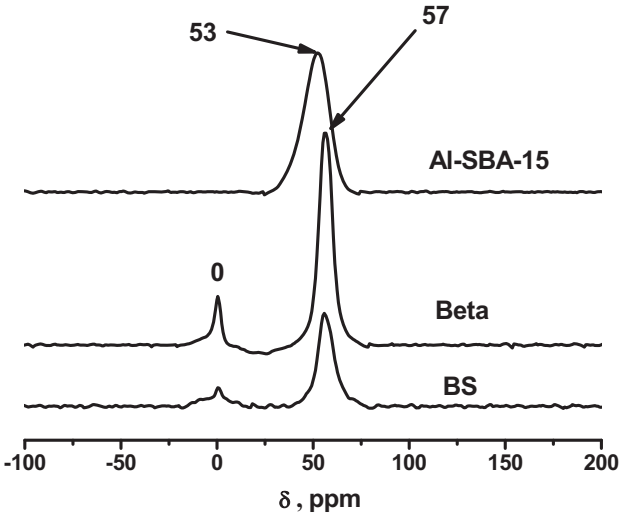

Fig. 11. ^{27}Al MAS NMR spectra of zeolite Beta, BS, and Al-SBA-15 samples.

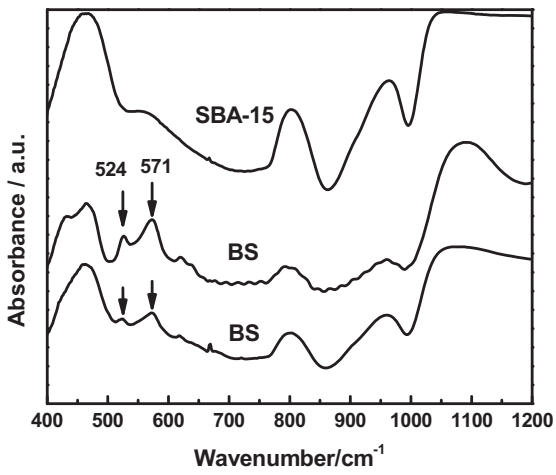

Fig. 12. FTIR spectra of SBA-15, BS, Beta samples.

Table 2
Amounts of Brönsted and Lewis acid sites determined by pyridine-FTIR of the catalysts.

Catalysts	200 °C[a]			350 °C[a]		
	Amount of acid sites/(μmol g^{-1})			Amount of acid sites/(μmol g^{-1})		
	L	B	L+B	L	B	L+B
NiMo/BS	539	51	590	431	34	465
NiMo/SBA-15	335	–	335	198	–	198
NiMo/Beta	677	98	774	510	98	608
NiMo/Al_2O_3	358	–	358	221	–	221

[a] Degassed at 200 °C and 350 °C.

hydrogen-bonded pyridine, bands at 1450, 1610 and 1622 cm^{-1} to strong Lewis acid site-bound pyridine, the band at 1575 cm^{-1} to weak Lewis acid site-bound pyridine and bands at 1546 and 1639 cm^{-1} to pyridinium ion ring vibration due to pyridine bound to Brönsted acid sites. The band at 1492 cm^{-1} is assigned to pyridine associated with both Brönsted and Lewis acid sites. The NiMo/Al_2O_3 and NiMo/SBA-15 catalysts exhibit typical signals due to hydrogen-bonded pyridine at 1596 cm^{-1} and pyridine adsorbed on Lewis acid sites (absorption peaks at 1446, 1575, 1609, 1622, and 1492 cm^{-1}). No Brönsted acid site is observed in the spectra of the NiMo/Al_2O_3 and NiMo/SBA-15 catalysts due to the absence of absorption band at 1546 cm^{-1}. In contrast, bands at 1546 and 1639 cm^{-1} are observed in the spectra of the NiMo/Beta and NiMo/BS catalysts, suggesting the existences of Brönsted acid sites in these samples. These results demonstrate that the BS-supported NiMo catalyst exhibits an acidic property similar to that of the Beta-supported NiMo catalyst, and that acidic property is different from those of NiMo/SBA-15 and NiMo/Al_2O_3 catalysts. This is probably because both Beta- and BS-supported catalysts possess framework aluminum species (Fig. 11) which are responsible for the Brönsted acid sites.

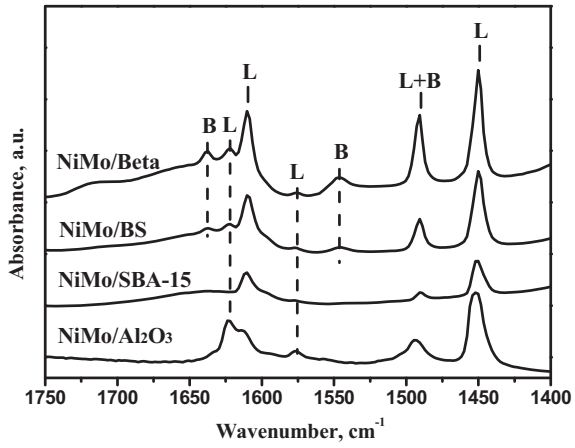

Fig. 13. FTIR spectra of pyridine adsorbed on NiMo/Al_2O_3, NiMo/SBA-15, NiMo/BS and NiMo/Beta after degassing at 200 °C.

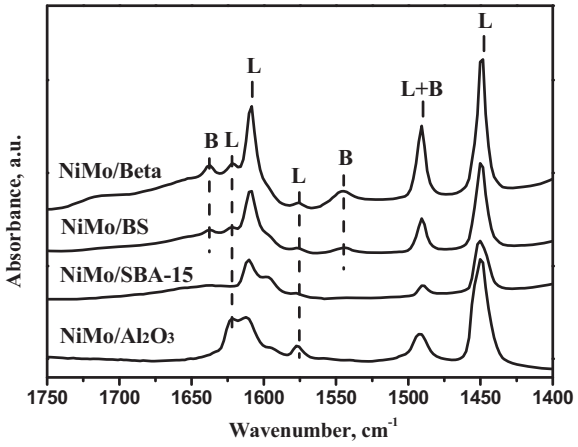

Fig. 14. FTIR spectra of pyridine adsorbed on NiMo/Al_2O_3, NiMo/SBA-15, NiMo/BS, NiMo/Beta after degassing at 350 °C.

Table 2 lists the acid strength distributions and the acid quantity of the catalysts. These results are calculated from the IR spectra that were collected on the catalysts with pyridine adsorption after being degassed at 200 °C and 350 °C (the total amount of acid sites were determined by the pyridine adsorption IR spectra after degassing at 200 °C, the amount of medium and strong acid sites were determined by the IR pyridine adsorption spectra after degassing at 350 °C). It is clear that after degassing at 200 °C the total amount of acid sites (B + L) of the NiMo/BS catalyst is much higher than that of NiMo/SBA-15 and NiMo/Al_2O_3 catalysts, and a slightly lower than that of NiMo/Beta catalyst. This distinction is more notable (more than two times) for the amounts of medium and strong acid sites (B + L after degassing at 350°C). Compared with NiMo/BS catalyst, NiMo/Beta catalyst possesses more strong acid sites especially for the Brönsted acid sites. All the Brönsted acidity in Beta is contributed by the medium and strong acid sites. There is a significant proportion of weak Brönsted acid sites in NiMo/BS, although the total number of Brönsted acid sites is less than that of NiMo/Beta. This may be due to the distinctive Al chemical environment and the presence of extra framework Si–O–Al species in the BS sample (Fig. 11).

3.6. Catalytic performance for the HDS of DBT

The catalytic performance of the supported NiMo catalysts was examined on the HDS of DBT which is one of the typical molecule and one of the most refractory sulfur compounds

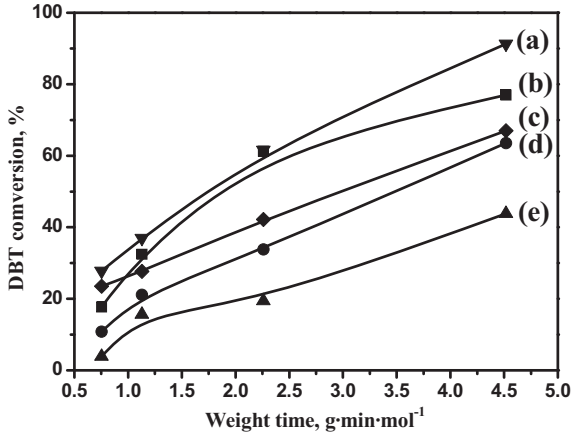

Fig. 15. Conversion of DBT in the HDS reaction over supported NiMo catalysts with various supports. (a) BS, (b) Al_2O_3, (c) Al-SBA-15, (d) SBA-15, and (e) Beta.

in gas oil. The BS-supported NiMo catalyst showed the highest DBT conversion at all weight times, and its DBT conversion was about 1.6 times as much as that over the Al_2O_3-supported catalyst at $\tau = 0.75$ g min mol^{-1} (Fig. 15). The SBA-15-supported catalyst exhibited a lower DBT conversion than the BS-supported one at all weight times, although it had larger surface area and pore volume (Table 1). This is probably due to the relatively weak acidity of the pure silica material SBA-15 (Table 2). The Beta-supported NiMo catalyst exhibited the lowest conversion although it had the most acid sites (Table 2). Although Al-SBA-15-supported NiMo catalysts showed a little higher DBT conversion than SBA-15 supported one, they also had the lower activities than BS-supported one (Fig. 15).

The acid properties of catalysts had a large effect on the catalytic performances of the HDS catalysts. Supports or catalysts with proper acid distributions can improve the conversions of DBT and/or 4,6-DMDBT [10,11]. One of explanations was that acidity helped to improve the reaction rates of dealkylation and isomerization of alkyl substituents, which might favor the transformation of the refractory components into more reactive species and thus accelerated HDS process [11]. Moreover, acidic supports could also promote the catalytic activity by the creation of a second hydrogenation pathway through spillover of hydrogen atoms from the metal particles to the aromatic sulfur-containing molecules that were adsorbed on acid sites in the vicinity of the metal active sites [32]. In this paper, however, NiMo/Beta catalyst exhibited the lowest activity although it had the highest amounts of acid sites, which indicated that the pore size also played an important role in DBT HDS reaction. Mesoporous materials with large pores can eliminate the diffusion resistance and enhance the accessibility of the active sites to reactant molecules. So mesoporous materials MCM-41 and SBA-15 have been employed as catalyst supports for the HDS of DBT or 4,6-DMDBT and exhibited good catalytic performances [3,9]. However, pure silica mesoporous materials possessed electronically neutral frameworks and were devoid of Brönsted and Lewis acid sites. Micro-mesoporous material BS not only combined the superiorities of pore structure (as the mesoporous materials) but also possessed large amounts of acid sites (like zeolite), those properties made BS to be a good catalyst support for DBT HDS reaction.

4. Conclusions

In this study, micro-mesoporous composite material BS was successfully synthesized. The characterization results showed that the composite material possessed the same mesoporous structure as SBA-15 and contained Beta zeolite crystals simultaneously. N_2 adsorption result indicated that BS material had large uniform pore size, large pore volumes and surface areas of typical mesoporous materials. BS-supported NiMo catalyst was prepared and characterized. The ordered mesoporous structure of BS remained after the impregnation of Ni and Mo. BS-supported NiMo catalyst exhibited more and stronger acidic sites than the pure silica material SBA-15-supported one.

The catalytic testing results revealed that NiMo/BS had the highest DBT HDS activity among all the studied catalysts, and the DBT conversion on NiMo/BS was about 1.6 times as much as that on NiMo/Al_2O_3 at weight time of 0.75 g min mol^{-1}. The high activity of BS-supported catalyst might be attributed to the combination of open mesoporous structure and the large amounts of acid sites.

Acknowledgements

The authors acknowledge the financial supports from National Natural Science Foundation of China (no. 20876173, 21073235 and 20833011), Ministry of Education key project of China (no. 31).

References

[1] C. Song, X. Ma, Appl. Catal. B 41 (2003) 207.
[2] A. Duan, G. Wan, Z. Zhao, C. Xu, Y. Zheng, Y. Zhang, T. Dou, X. Bao, K. Chung, Catal. Today 119 (2007) 13.
[3] U.T. Turaga, C. Song, Catal. Today 86 (2003) 129.
[4] M.J.B. Souza, B.A. Marinkovic, P.M. Jardim, A.S. Araujo, A.M.G. Pedrosa, R.R. Souza, Appl. Catal. A 316 (2007) 212.
[5] D. Zhao, J. Feng, Q. Huo, N. Melosh, G. Fredrickson, B. Chmelka, G. Stucky, Science 279 (1998) 548.
[6] D. Zhao, Q. Huo, J. Feng, B.F. Chmelka, G.D. Stucky, J. Am. Chem. Soc. 120 (1998) 6024.
[7] A. Sampieri, S. Pronier, J. Blanchard, M. Breysse, S. Brunet, K. Fajerwerg, C. Louis, G. Pérot, Catal. Today 107–108 (2005) 537.
[8] L. Vradman, M.V. Landau, M. Herskowitz, V. Ezersky, M. Talianker, S. Nikitenko, Y. Koltypin, A. Gedanken, J. Catal. 213 (2003) 163.
[9] G.M. Dhar, G.M. Kumaran, M. Kumar, K.S. Rawat, L.D. Sharma, B.D. Raju, K.S.R. Rao, Catal. Today 99 (2005) 309.
[10] Y. Sun, R. Prins, Angew. Chem. Int. Ed. 47 (2008) 8478.
[11] G. Pérot, Catal. Today 86 (2003) 111.
[12] Z.Y. Wu, H.J. Wang, T.T. Zhuang, L.B. Sun, Y.M. Wang, J.H. Zhu, Adv. Funct. Mater. 18 (2008) 82.
[13] T. Klimova, J. Reyes, O. Gutiérrez, L. Lizama, Appl. Catal. A 335 (2008) 159.
[14] W. Hu, Q. Luo, Y. Su, L. Chen, Y. Yue, C. Ye, F. Deng, Micro. Meso. Mater. 92 (2006) 22.
[15] Y. Han, F.S. Xiao, S. Wu, Y. Sun, X. Meng, D. Li, S. Lin, F. Deng, X. Ai, J. Phys. Chem. B 105 (2001) 7963.
[16] K. Egeblad, C.H. Christensen, M. Kustova, C.H. Christensen, Chem. Mater. 20 (2008) 946.
[17] J. Čejka, S. Mintova, Catal. Rev. -Sci. Eng. 49 (2007) 457.
[18] Y. Liu, W. Zhang, T.J. Pinnavaia, J. Am. Chem. Soc. 122 (2000) 8791.
[19] S. Zeng, J. Blanchard, M. Breysse, Y. Shi, X. Su, H. Nie, D. Li, Appl. Catal. A 298 (2006) 88.
[20] M. Choi, H.S. Cho, R. Srivastava, C. Venkatesan, D.H. Choi, R. Ryoo, Nat. Mater. 5 (2006) 718.
[21] M. Egorova, R. Prins, J. Catal. 225 (2004) 417.
[22] K. Soni, B.S. Rana, A.K. Sinha, A. Bhaumik, M. Nandi, M. Kumar, G.M. Dhar, Appl. Catal. B 90 (2009) 55.
[23] T.W. Kim, F. Kleitz, B. Paul, R. Ryoo, J. Am. Chem. Soc. 127 (2005) 7601.
[24] Y. Wan, D. Zhao, Chem. Rev. 107 (2007) 2821.
[25] H. Shimada, T. Sato, Y. Yoshimura, J. Hiraishi, A. Nishijima, J. Catal. 110 (1988) 275.
[26] J.S. Beck, J.C. Vartuli, W.J. Roth, M.E. Leonowicz, C.T. Kresge, K.D. Schmitt, C.T.W. Chu, D.H. Olson, E.W. Sheppard, J. Am. Chem. Soc. 114 (1992) 10834.
[27] E. Lippmaa, A. Samoson, M. Magi, J. Am. Chem. Soc. 108 (1986) 1730.
[28] Y. Yue, A. Gédéon, J.L. Bonardet, J.B.D. Espinose, J. Fraissard, N. Melosh, Chem. Commun. 1999 (1999) 1967.
[29] T. Kataoka, J.A. Dumesic, J. Catal. 112 (1988) 66.
[30] D. Zhang, A. Duan, Z. Zhao, G. Wan, Z. Gao, G. Jiang, K. Chi, K.H. Chuang, Catal. Today 149 (2010) 62.
[31] B. Chakraborty, B. Viswanathan, Catal. Today 49 (1999) 253.
[32] S.D. Lin, M.A. Vannice, J. Catal. 143 (1993) 539.